# Polymer Assisted Transfer of Graphene onto Semiconductor Substrates

Physics: Bachelor's Degree Project

Project Duration: 2 Months

Division of Synchrotron Radiation Physics, Lund University

Written by Jonathan Frisby

Supervised by Anders Mikkelsen

Cosupervised by S. Fatemeh Mousavi


LUND UNIVERSITY

**Department of Physics**

# Contents

# Abstract

Since first being isolated in 2004, Graphene has been researched heavily because of its unique properties. Recently, interest has grown in graphene/semiconductor heterostructures. In this work, the transfer of graphene through the use of cellulose acetate butyrate (CAB) polymer is studied. CAB assisted transfer of graphene to indium arsenide (InAs) (111)B and undoped gallium arsenide (GaAs) (110) wafers is performed, and the CAB is removed by submerging the samples in acetone. The resulting graphene/semiconductor heterostructures are examined using optical microscopy and scanning tunneling microscopy (STM).

Optical microscopy revealed that a significant amount of polymer residues remained on the surfaces of the semiconductors following the treatment with acetone, although these residues were only apparent in the locations of the transfers. STM images of the clean areas of the InAs wafers confirmed that minimal polymer residues were present outside the transfer site. Using STM measurements from one of these areas, the interplanar distance for InAs(111)B planes was estimated to be 3.56 Å, very nearly the value of 3.50 Å that is predicted by theory. STM at the locations of the transfers had drastically reduced image quality, likely due to polymer residues adhering to the STM tip. Future studies are recommended involving the use of polymethyl-methacrylate (PMMA) in place of CAB or using ethyl acetate to dissolve the CAB before treating the samples with acetone.

# Acknowledgments

First and foremost, I would like to thank my supervisor, Anders Mikkelsen, and co-supervisor, S. Fatemeh Mousavi, for giving me the chance to work on this ambitious project, and never ceasing to help me along the way.

I would also like to thank Jose Caridad for providing countless useful insights into the transfer process.

Vidar Flodgren and Yen-Po Liu, I would like to thank you both for taking the time to teach me about lithography, and for just being generally helpful.

I would like to express my gratitude to the staff of the Lund Nano Lab for providing tools and assistance that made this project possible.
I would like to thank my dear friend, Jim Klintrup, for keeping me sharp and motivated, not just during this experiment, but throughout the entire bachelor's program.

And last, but not least, thank you to my wife, my family, and all my friends who have supported me throughout this degree.

# List of Abbreviations

**BCC:** Body-centered Cubic
**CAB:** Cellulose Acetate Butyrate
**CVD:** Chemical Vapor Deposition
**FCC:** Face-centered Cubic
**FLG:** Few-layer graphene
**GaAs:** Gallium Arsenide
**InAs:** Indium Arsenide
**InSb:** Indium Antimonide
**IPA:** Isopropanol
**LDOS:** Local Density of States
**LED:** Light Emitting Diode
**PMMA:** Polymethyl-methacrylate
**RMS:** Root Mean Square
**SC:** Simple Cubic
**Si:** Silicon
**$SiO_2$:** Silicon Dioxide
**STM:** Scanning Tunneling Microscopy

# 1 Introduction

Graphene is a two-dimensional allotrope of carbon in which the carbon atoms are arranged in a hexagonal pattern [1]. Graphene was first isolated in 2004 by Novoselov and Geim by using household clear tape to cleave flakes from graphite crystals [2]. Quickly, research into graphene accelerated because of its many unique properties. For example, graphene is a so called zero bandgap semiconductor in which the valence and conduction bands intersect at what is called the Dirac point [3]. The electronic structure of graphene causes its charge carriers to behave like massless, relativistic Dirac fermions [3, 4]. The electronic and optoelectronic properties of graphene make it a good candidate as a standalone material for devices, but there is also interest in graphene/semiconductor heterostructures.

Semiconductor materials have, for decades, formed the basis for most electronic devices. Light emitting diodes, transistors, and many other components all rely on the small bandgaps present in semiconductor materials for their operation [5]. When two materials are placed in contact, the electron dispersion bands "bend" at the interface [6]. Thus, graphene/semiconductor heterostructures have unique band structures that depend on the semiconductor material used and the geometry of the heterostructure [3, 6]. Recently, there has been a large amount of research into developing and characterizing such heterostructures.

The purpose of this work is to perform polymer assisted transfers of graphene onto InAs(111)B and GaAs(110) using a polymer called cellulose acectate butyrate (CAB), and to perform scanning tunneling microscopy (STM) on the resulting heterostructures. In this way, it is possible to become familiar with the transfer process, and to see what effect the CAB polymer has on the InAs and GaAs substrates. This will aid future experiments that will involve the characterization of heterostructures composed of graphene and InAs or GaAs nanowires.

# 2 Scientific Background

## 2.1 Properties of Graphene

As was mentioned in the introduction, graphene exhibits numerous properties that have made it a prime candidate for research in the past decade. One property that distinguishes graphene from other materials is its conductivity, $\sigma$, in the limit of few charge carriers, $n$. In all other known materials, $\sigma$ vanishes at low $n$ [3, 7]. This causes a transition at low temperature from metallic behavior, to that of an insulator. Graphene has an exceptionally low conductivity, approaching $\sigma = 4e^2/h$ per charge carrier in the limit of low $n$, where $e^2$ is the fundamental charge squared, and $h$ is Planck's constant. Still there is no evidence of a transition from metal to insulator in graphene even at temperatures as low as 4 K [7].

Another property of graphene that differentiates it from other materials is its relatively high charge carrier mobility, $\mu$. Undoped indium antimonide (InSb a III-V semiconductor) at room temperature has a $\mu \approx 77,000$ cm$^2$/Vs (which is already remarkably high), whereas graphene at room temperature has been shown to have a charge carrier mobility as high as 230,000 cm$^2$/Vs with $n$ as high as $2\times10^{11}$ cm$^{-2}$ [7, 8]. The drift velocity of charge carriers in a material is directly proportional to $\mu$. Therefore, graphene based devices have the potential to carry electrical signals much faster than a standalone semiconductor device. This is valuable in ordinary devices, but even more important for transistor technology. Early research indicates that using a layer of graphene as gate in metal-oxide semiconductor field effect transistors, can increase the switching rate of the transistor by a factor of 30. By improving the switching rate of transistor technology, it will be possible to create faster computer processors, as the maximum clock speed of a processor is limited by the switching rate of the transistors [3].

Graphene's optical properties also make it an interesting candidate for research. Graphene is known to absorb light in a range of wavelengths extending from sub-infrared to ultraviolet. In this regime, graphene absorbs approximately 2.3% of incident light [3]. When absorption of a photon occurs, an electron-hole pair is formed. Typically the electron and hole recombine on a timescale of several picoseconds, however; by applying an external electrical bias, the electon and hole can be separated, inducing a photocurrent [3, 5]. Combined with the high drift velocity of charge carriers, graphene has the potential to create photodetectors that function faster than the ubiquitous semiconductor photodetectors.

## 2.2 Production of Graphene

There are a variety of methods for producing graphene that have been developed in the years since it was first isolated. The earliest of these methods involved the isolation of graphene from bulk graphite, but today, production of graphene from non-graphitic sources is becoming more common [9]. Although this experiment uses the method that led to the original isolation of graphene, micromechanical cleavage from graphite using adhesive tape, a number of other techniques are presented here.

Micromechanical cleavage of graphene is performed by placing graphite crystals onto the adhesive side of clear tape. The tape is folded together around the graphite crystals and then peeled apart. When this is done, thinner flakes of graphite are exfoliated from the surfaces of the crystals. This is repeated several times as desired, producing successively thinner flakes. Eventually Few-Layer Graphene (FLG) and even single layer graphene are obtained [1, 9, 10]. The tape is then attached to a wafer made of silicon (Si) with a layer of silicon dioxide ($SiO_2$), and then removed, in the process leaving behind some of the flakes that have been exfoliated [9, 10]. The thin layer of $SiO_2$ is used because when the FLG or graphene flakes are present on the surface of the layer, the additional thickness causes thin film interference that enhances the optical contrast of the flakes with the surrounding areas of the wafer [9, 11]. This makes it possible to identify graphene flakes in an optical microscope [9, 10, 11]. Devices can then be built directly on the graphene on this wafer, or the graphene can be transferred to another substrate [9]. An illustration of this process is shown in figure 1. While other techniques are capable of producing larger quantities of graphene more quickly and with less human involvement, micromechanical cleavage remains popular because it does not require highly specialized tools and can produce relatively large flakes of graphene with clean surfaces [3, 9, 10].

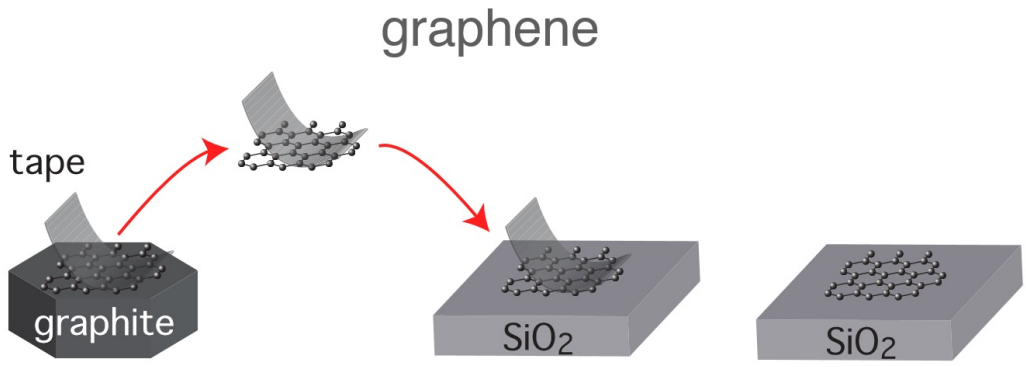


Figure 1: An illustration of the production of graphene using tape, and the subsequent deposition onto $Si/SiO_2$. Image from Philip Hofmann's book *Solid State Physics: An Introduction* [5].

Recently Chemical Vapor Deposition (CVD), in which heated metal surfaces held under vacuum are exposed to hydrocarbons which subsequently lose their hydrogen and adhere to the metal surface, has become the most popular and efficient method for producing graphene [3, 9]. In 2009, researchers were able to grow sheets of graphene with side lengths approaching 75 cm, on a copper substrate [12]. A challenge of CVD is that while large sheets of graphene are produced, the size of the individual crystal domains is often relatively small because several graphene "seeds" form on the surface of the metal and then grow into each other with different orientations [9]. In 2014, researches oxidized a copper surface before performing CVD. This limited the number of potential nucleation sites for graphene, and the researchers were able to grow a single graphene crystal with a diameter of approximately 1 cm [13].

A variety of less common techniques for producing graphene also exist. In liquid phase mechanical exfoliation, graphite crystals are mixed with a solvent and sonicated in order to exfoliate single sheets of graphene [9, 14]. The resulting suspension is then centrifuged in order to remove the unexfoliated graphite [9, 15]. Graphene has also been produced in the form of nanoribbons, by exposing aromatic precursors to hot gold [16]. Still, more methods exist for the the production of graphene, and research into the topic is accelerating [9].

## 2.3 Polymer Assisted Transfer of Graphene

Once graphene is produced, it is often desired to transfer the graphene to another substrate. A common method for transferring graphene involves depositing a layer of polymer on the graphene flakes. In the case of graphene produced by micromechanical cleavage, the flakes can be spin coated [1] with polymer while on the $Si/SiO_2$ wafer they are identified on. The polymer can then be cut in the desired area, transferred to a target, and the polymer is dissolved in acetone [17, 18]. CVD grown graphene can be coated with polymer, and the growth substrate, often copper or nickel, can be etched away using ferric chloride [1, 17]. Again, the polymer with graphene flakes attached, is transferred to the target, and the polymer is dissolved in acetone. Common polymers for this application are polymethyl-methacrylate (PMMA) and the CAB polymer used in this experiment [17]. Research has shown that CAB leaves fewer residues on graphene than PMMA [19].

[1] Spin coating is a process in which thin layers of materials are deposited onto flat substrates. The substrate is held onto a platform capable of rotation, usually using light vacuum beneath the substrate, and the desired liquid is dropped onto the substrate. The rotating platform is switched on and the centrifugal force causes the material to spread nearly uniform across the surface of the substrate.

## 2.4 Crystal Structure

Many solids form crystals where the atoms of the solid are arranged in a regularly-spaced, periodic fashion. One key concept for crystals is the Bravais lattice, the lattice of points and position vectors that has the form [5, 20]:

$$\vec{R} = m_1\vec{a}_1 + m_2\vec{a}_2 + m_3\vec{a}_3 \tag{1}$$

The concept of the primitive unit cell is also important. The primitive unit cell is the smallest repeating unit of a crystal that has the symmetry of the crystal structure [5, 20]. A basis of atoms, and a Bravais lattice, can describe any crystal structure [5]. Examples of common crystal structures are simple cubic (SC), with atoms situated at the corners of a cube, body-centered cubic (BCC), a SC structure with an additional atom at the center of the cube, and the face-centered cubic (FCC), a SC structure with additional atoms at the center of each face of the cube. More complex structures also exist. InAS and GaAs are two crystalline semiconductor materials that are used in this experiment. Both of these materials have the zincblende structure, in which two FCC structures composed of the different atoms are interlocked [21]. Figure 2 shows an illustration of the zincblende unit cell.

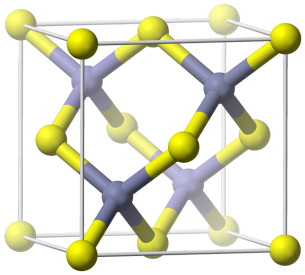

Figure 2: A public domain image showing the zincblende unit cell [22].

Another key concept in understanding crystals are Miller indices. Miller indices describe a specific plane within a crystal. To determine the Miller indices of a plane, the procedure is as follows:

1. Find the intercepts of the planes with the axes in terms of the lattice vectors.
2. Take the reciprocal of these numbers.
3. Reduce all these numbers to their lowest integer forms [5, 20].

Miller indices are typically written in the form $(h, k, l)$. Figure 3 shows a FCC crystal with the (001) surface highlighted.

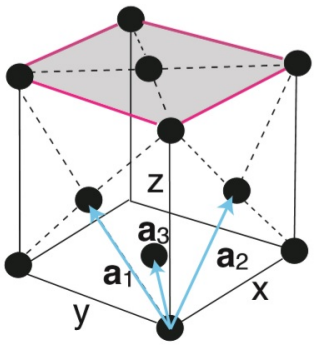


Figure 3: An image of a FCC crystal with the Bravais lattice vectors indicated in blue and the (001) surface highlited in gray. Image reproduced from P. Hofmann's book *Surface Physics* [20]

The InAs wafers used in this experiment have the (111)B surface exposed. The B indicates that the lattice terminates with arsenic atoms, as (111) planes in zincblende structures will expose one of the two atoms that the material is made of [21]. InAs(111)B has a characteristic, hexagonal structure with triangular islands, and smaller defects that appear as bright spots and are believed to be arsenic trimers and oxides [23]. The GaAs wafers used in the experiment have the (110) surface exposed. This is of particular importance, as nanowires with a zincblende structure tend to have (110) facets exposed [24]. Since the ultimate goal is to later use this transfer process to create graphene/nanowire heterostructures, experiments with this surface may provide insight that will aid future experiments.

If the structure of a crystal is known along with the so called lattice constant, a measure of the physical dimension of the primitive unit cell, then it is possible to determine the spacing of planes with given Miller indices. For a cubic crystal with latice constant, $a$, the interplanar spacing, $d$, for planes with Miller indices $(hkl)$ can be determined from the formula [5, 20]:

$$\frac{1}{d^2} = \frac{h^2 + k^2 + l^2}{a^2} \tag{2}$$

The lattice constants of InAs and GaAs are 6.06 Å and 5.65 Å respectively [23, 25]. Using equation (2), the interplanar spacings for InAs (111)B and GaAs (110) are calculated to be 3.50 Å and 4.00 Å respectively.

## 2.5 Scanning Tunneling Microscopy

STM is a form of scanning probe microscopy, first realized by G. Binning et al in 1982 [26]. In STM an atomically sharp metal tip is scanned very close to the surface of a sample. When the tip is brought close to the surface of a sample, electrons can tunnel

from the sample to the tip. A voltage difference is applied between the sample and the tip, and the tunneling current, $I_t$, is recorded at numerous points during the scan. This tunneling current is then used to create an image of the sample. The tunneling current could be be dramatically influenced by the presence of gas molecules between the tip and the sample. As such, it is necessary that STM is performed under high vacuum. For example, the STMs used for this experiment were maintained at pressures of the order of $10^{-9}$ mbar. STMs are typically operated in two modes, constant current and constant height. In constant current mode, the height of the tip is adjusted constantly in order to maintain a constant tunneling current. In constant height mode, the tip is held a constant height and scanned across the sample. Constant height mode provides faster, and potentially higher resolution images of atomically flat surfaces, but risks crashing the tip if there are elevated surface features [5, 20].

STM provides not only information about the geometry of the sample, but also its electronic structure. Depending on the bias between the tip and sample, a certain local density of electron states (LDOS) is probed [5]. A common reason for a large change in LDOS from one position to another on a sample, is that atoms of different species are present in those positions. Consider for example, the GaAs(110) surface. This surface exposes both group III Ga atoms and group V As atoms. More electrons are available to tunnel from As, so even if the geometry of the sample were perfectly flat, contrast would still be expected between the Ga and As atoms because of the difference in LDOS.

## 2.6 Cleaning Procedures

Throughout the experiment, multiple steps are taken to clean the samples. One of the methods used is plasma ashing. In a plasma asher, the sample is exposed to a plasma of a highly reactive species, such as monoatomic oxygen or fluorine, while under vacuum. The plasma burns away organic materials on the surface, and attaches to and desorbs other inorganic impurities, which are then carried away by the vacuum system [27]. Additionally, after the samples are introduced into the STM they must undergo annealing and hydrogen cleaning. In this process, the samples are heated, while a hydrogen gas cracker exposes the sample to heated hydrogen. This is known to dramatically reduce the amount of oxides present on the sample [28], and is necessary after every time a sample is exposed to ambient conditions.

# 3 Method

In order to minimize contamination of the sample, these preliminary sample preparation steps were performed in a cleanroom at the Lund Nano Lab. The experiment began by preparing graphene flakes from graphite crystals using the same method as the original discoverers, mechanical exfoliation with clear tape. Pieces of clear tape approximately 10 cm in length were cut. A small amount of graphite crystals were emptied from a vial onto the middle of the adhesive side of the tape. The section of the tape surrounding the graphite crystals was carefully pushed together, being careful to not attach clean areas of the tape to each other. The tape was then opened and the section containing graphite was attached to a nearby clean area of the tape. This process of attaching the graphite containing sections to a clean area and then peeling open the tape was repeated several times across the length of the tape. Each time this was done, successively thinner flakes of graphite are cleaved from the crystals. After repeating this several times the section of the tape containing the most recently cleaved flakes was attached to a clean area of the tape, and the tape was not separated in order to avoid as much contamination to the graphene/graphite as possible during preparation of the $Si/SiO_2$ wafer.

A small piece of wafer, approximately 1 $cm^2$ in size, made of Si with a top layer 100 nm thick of $SiO_2$ was placed in a plasma asher. The plasma asher used monoatomic oxygen plasma to clean the surface of the wafer before depositing the graphene/graphite flakes onto it. The wafer was treated three times for 60 s each, while supplied with a pressure of 5 mbar of monoatomic oxygen. As soon as the plasma asher was cooled to a safe temperature, the $Si/SiO_2$ wafer was removed. The tape which contained the graphene/graphite flakes was opened, and the area that held the most recently cleaved flakes was attached to the $Si/SiO_2$. A pair of tweezers was rested on top of the tape in order to apply gentle pressure to the tape and ensure that there was good contact with the wafer. The tweezers were then used to hold the wafer in place while the tape was removed from the wafer. Now, the surface of the wafer was coated with graphene and graphite flakes as well as residues from the adhesive on the tape. Numerous $Si/SiO_2$ wafers were prepared with graphene and graphite flakes deposited onto them in this manner.

After the wafers were coated with the graphene/graphite, they were placed into a sample holder and removed from the cleanroom. The wafers were moved to a laboratory with an optical microscope that had adequate objectives for the identification of graphene flakes. Images of areas containing graphene were saved, being careful to note the position of the flake on the wafer in the file name. An example of one of these images is shown in figure 4. The wafers were then placed back into the sample holder and immediately returned to the cleanroom.

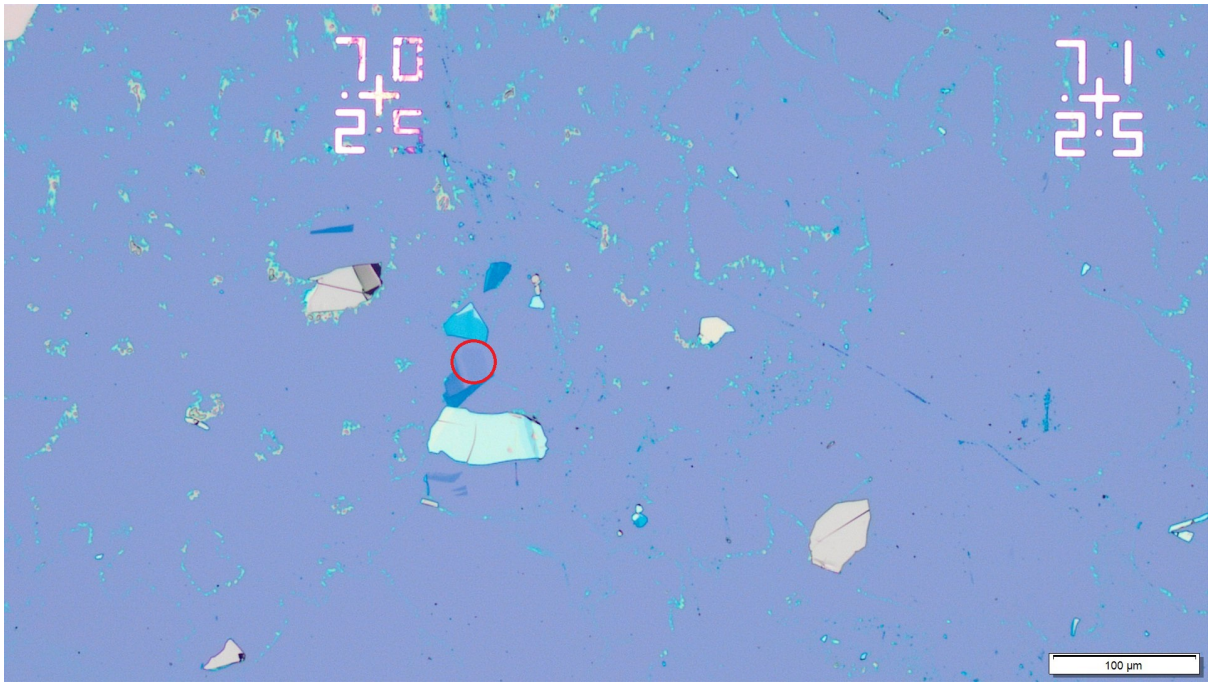


Figure 4: An optical microscope image of a $Si/SiO_2$ wafer following the deposition of graphene and graphite. A flake of graphene has been circled in red. The yellow and green streaks are residues from the adhesive on the tape. FLG is seen in dark blue, and larger graphite flakes appear yellow.

Now that the areas of interest on the wafers had been identified, the graphene and graphite flakes needed to be transferred to their final targets, InAs(111)B and GaAs(110) wafers. The $Si/SiO_2$ wafers that contained these flakes were spin coated with the CAB polymer. A pipette was used to place a few drops of the polymer onto the wafers, and the spin coater was set to spin at 1500 rpm for 60 s. The $Si/SiO_2$ wafers which were now coated with the polymer were then placed on a hot plate that was heated to 80 °C for 6 min. Now that the polymer was evenly distributed across the surface of the wafer, and well attached to the flakes, the hot plate was switched off and the wafers were removed from heat. Figure 5 shows a $Si/SiO_2$ wafer, with graphene and graphite deposited onto it, that has been spin coated with the CAB polymer.

Next, the wafers that were coated with the CAB polymer were examined under optical microscopes. The locations containing the flakes of interest were found in the microscopes. Tweezers were then placed between the wafer and the objective. When the tweezers were visible at the edges of the microscope image, the location of the tweezers above the chip was noted. A knife was then used to cut the polymer in this area. A pipette was used to put several drops of deionized water onto the wafers containing the cut polymer. Tweezers were used to pull at the edges of the cut in the polymer to allow the water to penetrate beneath the polymer. The CAB polymer is hydrophobic and $SiO_2$

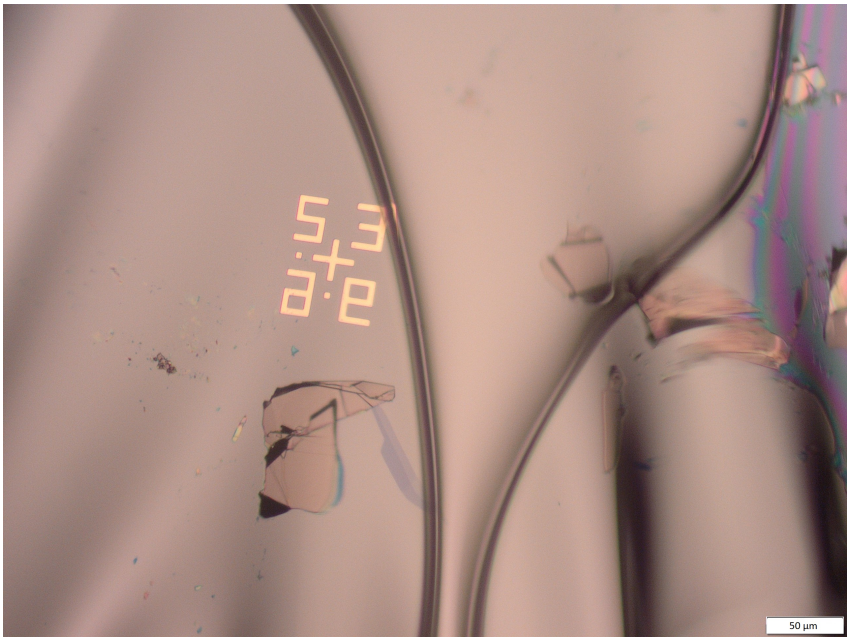


Figure 5: An optical microscope image of graphene and graphite flakes on $Si/SiO_2$, after being coated with the CAB polymer. Ripples can be seen in the image that are defects in the surface of the CAB that form when the solution containing the polymer is evaporated on the hot plate.

is hydrophilic, so the water that penetrates into the incisions will lift the polymer off of the wafer [18]. Soon the polymer was free from the $Si/SiO_2$ wafer and tweezers were used to place the small pieces of polymer containing the graphene and graphite flakes on the InAs and GaAs wafers.

Subsequently, the semiconductor wafers were placed on a hot plate that was heated to 80 °C for 60 s. The temperature was increased by 10 degrees until the hot plate warmed to the correct temperature and then allowed another 60 s. The temperature was repeatedly increased in this way until the temperature had reached 150 °C. At this point, the water from the previous step had completely evaporated and the polymer was well attached to the semiconductor wafers. Beakers containing isopropanol (IPA) and acetone were prepared. Each wafer was then submerged in acetone for some time, rinsed in the IPA, and then blown dry with nitrogen gas. One InAs wafer was cleaned in acetone for only two minutes (sample 1), another for two and a half hours (sample 2), and one InAs wafer and one GaAs wafer were left in the acetone overnight (samples 3 and 4 respectively). The acetone was used to dissolve the CAB polymer, and the IPA was used to remove acetone residue from the wafers. The wafers were now placed under the optical microscopes in the cleanroom so that "maps" could be created of the samples. These maps were used later as a reminder of which areas contained graphene and graphite flakes along with residue of the CAB polymer, and which areas were clean. An image from one of these maps is shown in figure 6 below.

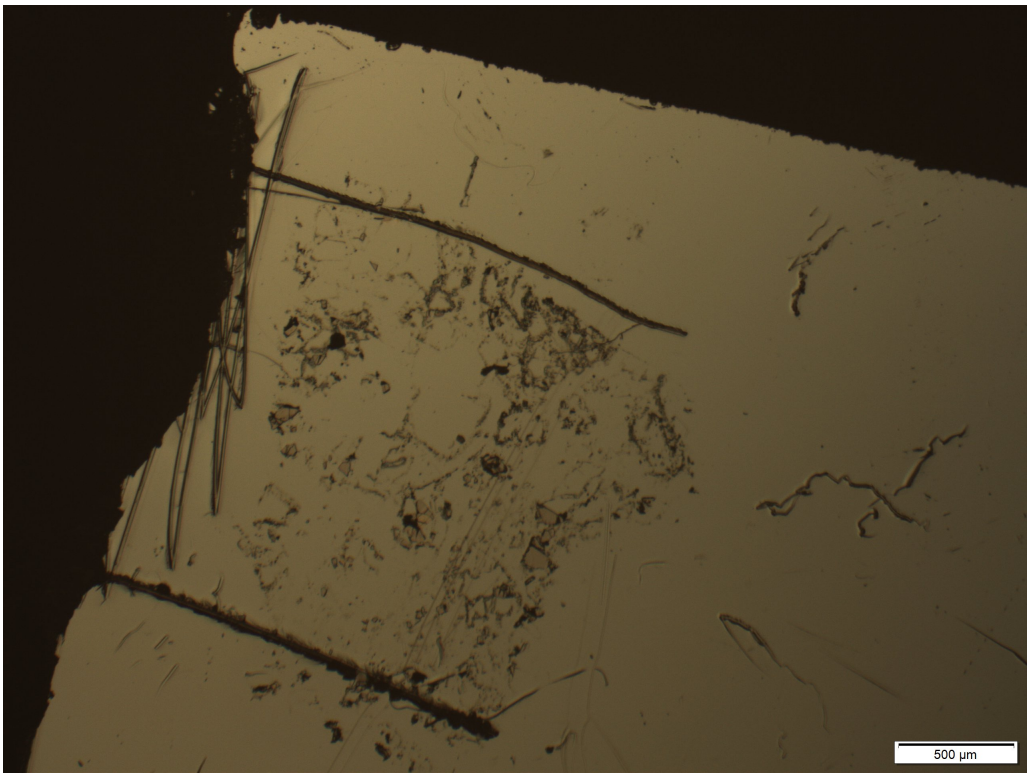


Figure 6: An optical microscope image of the InAs sample that was cleaned in acetone for two and a half hours. The area pictured was the location of the transfer. Scratches are seen that were made on the sample in order to aid finding the location in the STM. Polymer residues are visible as dark smears on the surface.

When there was available space in the STM, the samples were removed from the clean-room and mounted onto metal sample stages. Before the load/lock chamber was opened for the introduction of the samples, the valve connecting this chamber to the rest of the instrument was closed, to avoid exposing the entire instrument to ambient pressures. Then the turbo pump was turned off, and the valve to the mechanical pump was closed. When the speed of the turbo pump had reduced below 100 Hz, the load/lock chamber was opened, and then a sample was introduced. The load/lock chamber was then sealed, and the valve to the mechanical pump was opened. When the pressure in the load/lock chamber was of the order of $10^{-2}$ mbar, the turbo pump was switched on. When the pressure was of the order of $10^{-7}$ mbar, the valve to the rest of the instrument was opened.

The next step was to anneal the sample and perform atomic hydrogen cleaning in order to remove native oxides from the surface of the sample. When the samples are introduced they are locked into a retractable transfer rod. The transfer rod was extended into the chamber that contained the hydrogen source, and the sample stage was transferred to the manipulation arm in this chamber. The transfer rod from the load/lock chamber was withdrawn, and the valve connecting the load/lock chamber to the rest of the instrument

was closed. The ion pump connected to the main STM chamber was then switched off. The manipulation arm that now held the sample was connected to a current source that was used to anneal the sample through resistive heating. The current from the source was increased at a rate of 0.2 A/min, and the temperature of the samples were monitored using a pyrometer. The samples were annealed at approximately 420-430°C.

Additionally, the monoatomic hydrogen cleaning process was started. First, the pump for the cooling water was started, and the current source for the hydrogen cracker was switched on. The current was increased at a rate of 1 A/min, until the cracker had reached approximately 1700 °C. The thermocouple used to read the cracker's temperature was known to read a few hundred degrees lower than the actual temperature in this regime, so the decision was made to not exceed a measurement of 1400 °C on the display. When the desired temperature was reached, the variable leak valve for the hydrogen gas was opened until the pressure in the main STM chamber was $2\times10^{-6}$ mbar, and the shutter to the hydrogen cracker was opened. After about 30 min the hydrogen cleaning was complete, and the shutter to the cracker was closed along with the variable leak valve for the hydrogen gas. The currents used to heat the sample and the hydrogen cracker were decreased at rates of 0.2 A/min and 1 A/min respectively. After the temperature of the hydrogen cracker was below 100 °C, the cooling water was switched off, and the ion pump was restarted.

Finally, the samples were ready to be scanned. Using the transfer arm from the main STM chamber, the sample stages were moved from the manipulation arm to a position mounted just above the probe tip. The instrument was connected to a computer with the software *Matrix*. This software handled the data acquisition from the measurements, and also allowed for the control of the various scanning parameters such as scan speed, voltage difference between tip and sample, and image size. When data acquisition was complete, the resulting data was processed using *Gwyddion* a software for the visualization and analysis of data from scanning probe instruments.

# 4 Results and Discussion

This section summarizes the results obtained throughout the experiment. Images gathered from optical microscopy and STM on the graphene/InAs and graphene/GaAs samples are presented and analyzed.

## 4.1 Transfer of Graphene and Graphite to InAs(111)B

Three of the samples measured were graphene and graphite flakes transferred to InAs(111)B. The three samples all had the CAB polymer removed by washing the samples in acetone for different lengths of time. Sample 1 was washed for two minutes, Sample 2 was washed for 150 minutes, and Sample 3 was washed in acetone overnight. Optical microscope images of the location of the transfer and the "clean" area of sample 2 are shown in figure 7 and 8 respectively. An optical microscope image of the location of the transfer on sample 3 is also shown in figure 9.

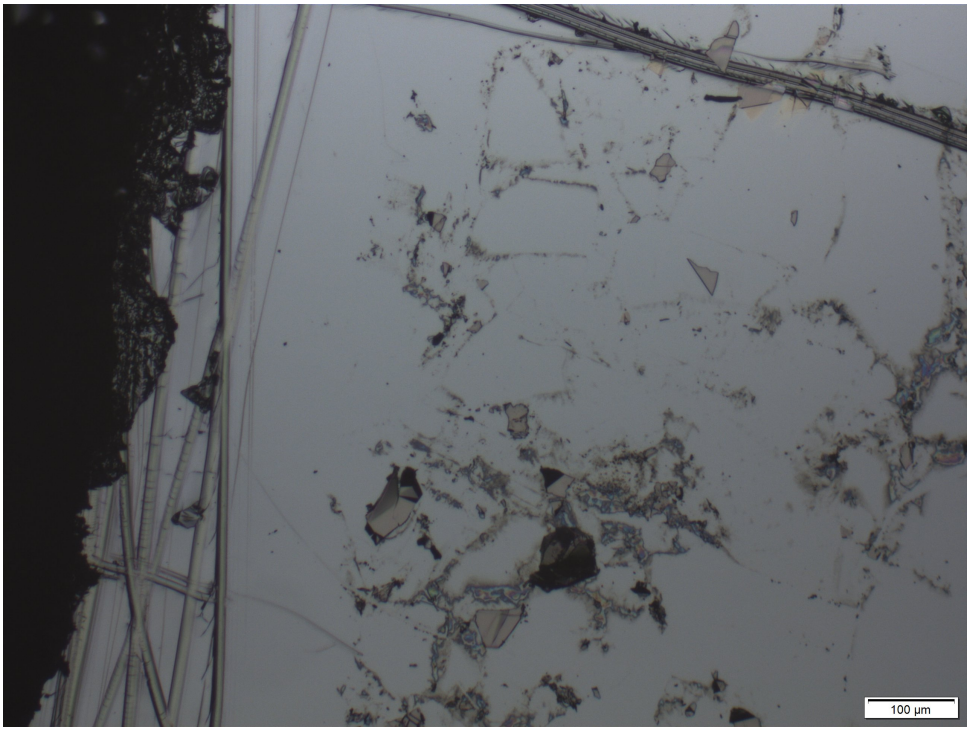


Figure 7: An optical microscope image of sample 2, at the location of the transfer, after dissolving away the CAB. At the top and left sides of the image scratches are visible that were made on the substrate in order to help position the graphene during the transfer.

From figures 7 and 9, it would appear that increasing the duration of exposure to acetone, when dissolving the CAB polymer, did not noticeably reduce the amount of polymer residue present on the samples. As evidenced by figure 8, the parts of the wafers that were not selected for the transfers appeared to be relatively clean of polymer residues.

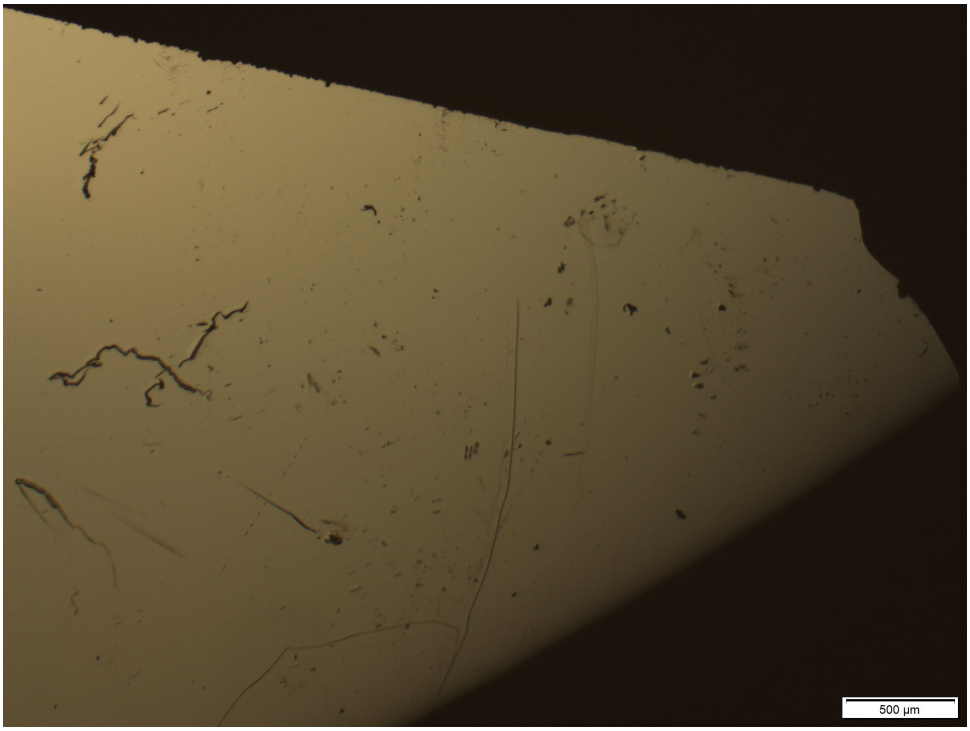


Figure 8: An optical microscope image of sample 2 in a "clean" area. Scratches and contaminants are visible.

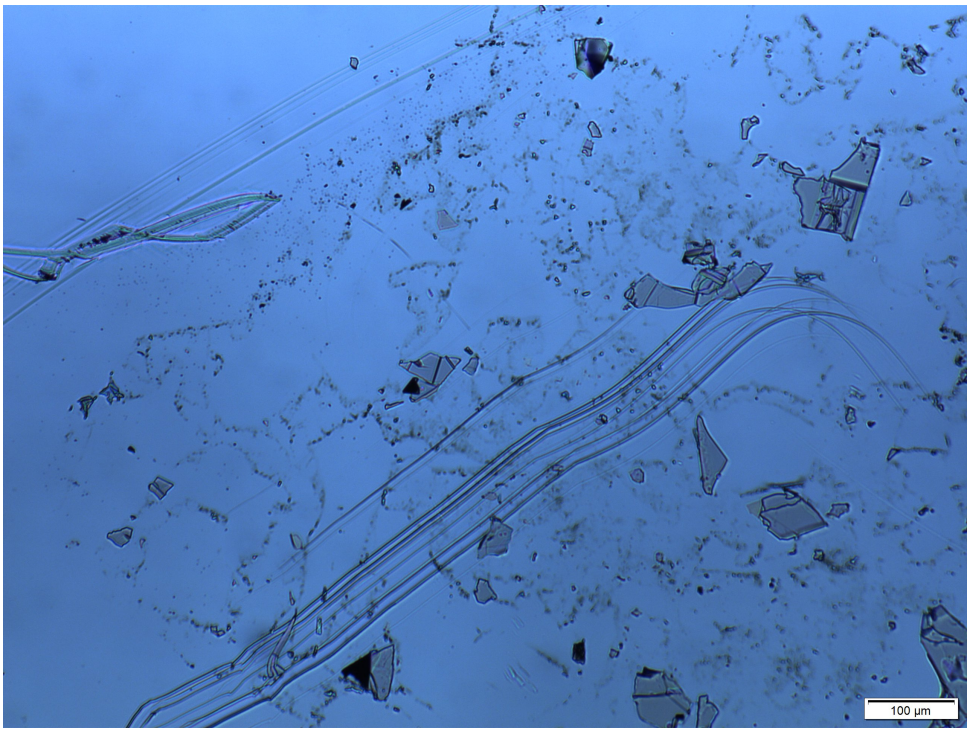


Figure 9: An optical microscope image of sample 3, at the location of the transfer, after dissolving away the CAB. The large streaks are believed to be scratches made by tweezers during the transfer process.

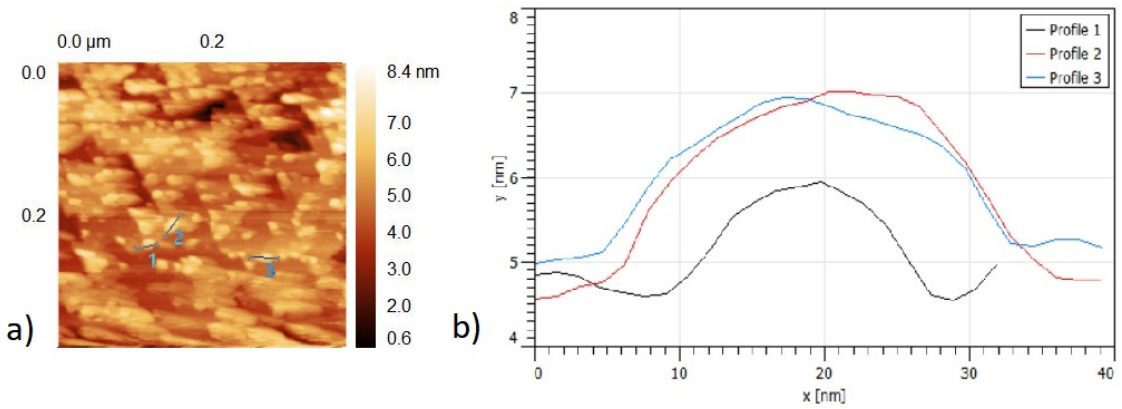


Figure 10: **(a)** An STM image taken from a clean area of sample 1. Image acquired using the following parameters: $V_{gap}$ = -1.5 V, loop-gain 1.5%, $I_t$ = 100 pA, 100.2 nm/s scan speed, 400 × 400 nm$^2$. **(b)** Data extracted from the line profiles taken over the bright spots seen on the clean InAs (111)B surface shown in figure 10 (a).

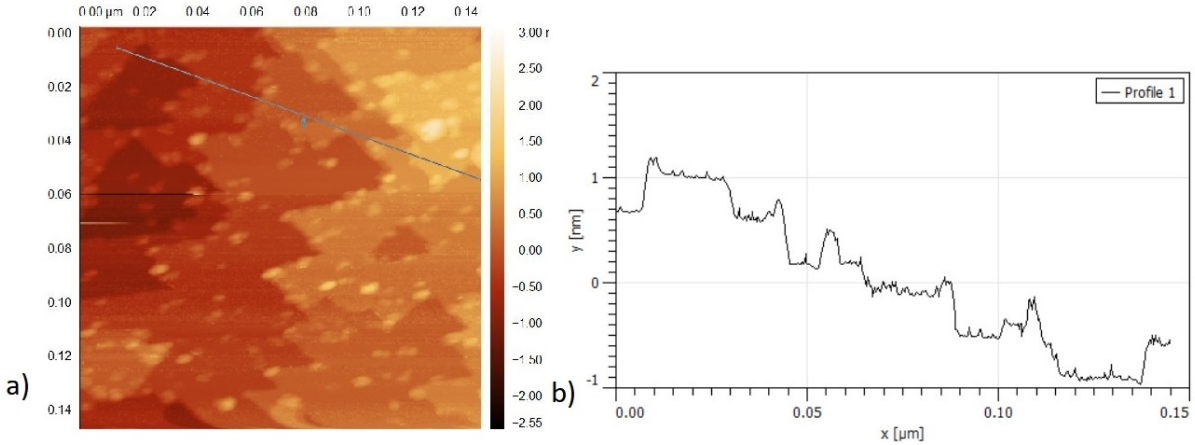


Figure 11: **(a)** An STM image taken from a clean area of sample 2. A line profile extracted from this image is indicated in gray. Image acquired using the following parameters: $V_{gap}$ = -0.7 V, loop-gain 0.8%, $I_t$ = 120 pA, 67.90 nm/s scan speed, 150 × 150 nm$^2$. **(b)** Data extracted from the line profile on the clean InAs(111)B surface shown in figure 11 (a). The average step height along this profile was found to be 3.56 Å.

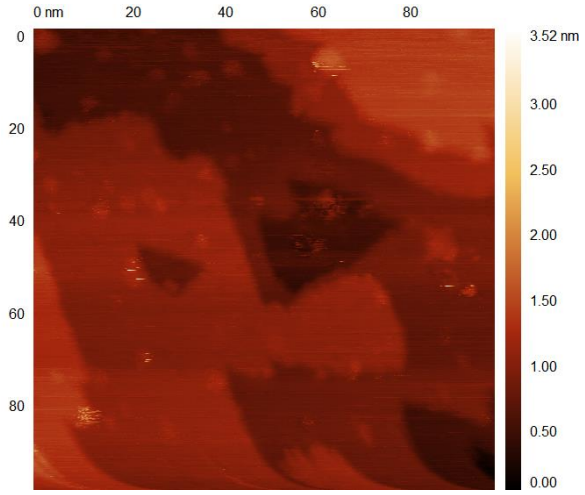


Figure 12: An STM image taken from a clean area of sample 3. Image acquired using the following parameters: $V_{gap}$ = -1 V, loop-gain 1%, $I_t$ = 100 pA, 95.06 nm/s scan speed, 100 × 100 $nm^2$.

Figures 10, 11, and 12 show STM images taken from clean areas on samples 1, 2, and 3, respectively. Figure 10 (b) shows the data from the line profiles extracted over the bright spots indicated in figure 10 (a). These bright spots are believed to be either oxides that have formed on the surface after the $H_2$ treatment or that were not removed by the treatment, or possibly residue from the CAB. These contaminants could be relatively large, with some approaching 30 nm in width and 3 nm in height. Figure 11 (b) contains a plot of the tip height along the line profile specified in figure 11 (a). The average step height calculated along this profile was 3.56 Å. This is near the value of 3.50 Å predicted by equation (2) as the distance between InAs(111)B planes, and confirmed in other experiments [23]. It is likely that if more profiles were considered in the average, this value would converge even closer to the expected value. The root mean square (RMS) surface roughness for the areas seen in figures 10, 11, and 12 were found to be 960.3 pm, 336.2 pm, and 258.8 pm, respectively. The surface roughness at the locations of the transfers decreased as the duration of the acetone washed increased. In this case, a higher surface roughness is most reasonably explained by the presence of residues from the CAB that spread to the areas surrounding the transfer location during the acetone bath. These STM measurements seem to confirm what was suspected from the optical microscope images, polymer residues are not present in significant quantities outside the location of the transfer.

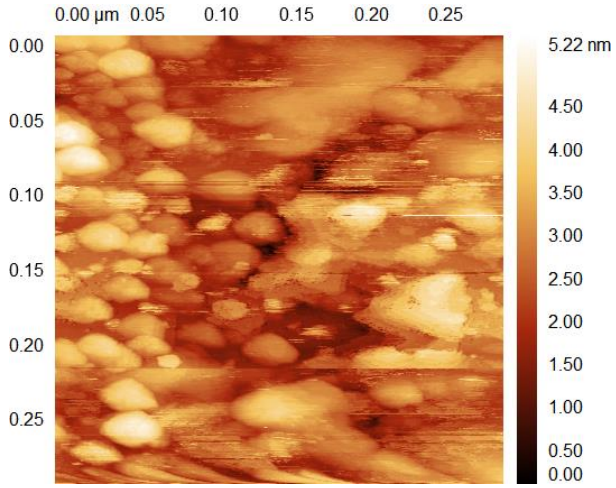


Figure 13: An STM image taken from the location of the transfer on sample 1. Image acquired using the following parameters: $V_{gap}$ = -1.5 V, loop-gain 1.5%, $I_t$ = 100 pA, 131.6 nm/s scan speed, 300 × 300 nm$^2$.

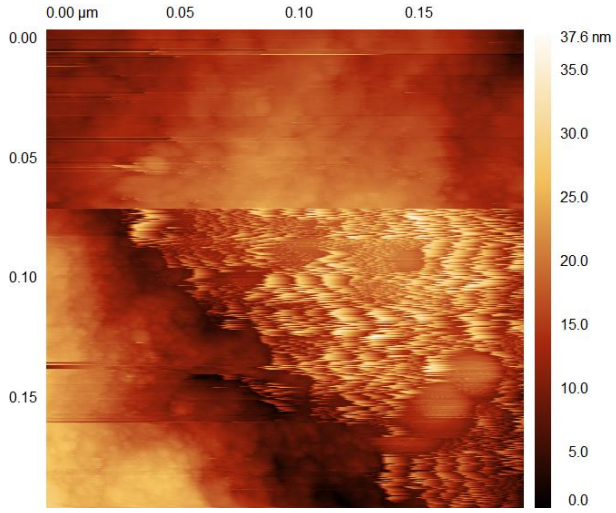


Figure 14: An STM image taken from the location of the transfer on sample 2. Image acquired using the following parameters: $V_{gap}$ = -0.7 V, loop-gain 0.8%, $I_t$ = 120 pA, 67.90 nm/s scan speed, 200 × 200 nm$^2$.

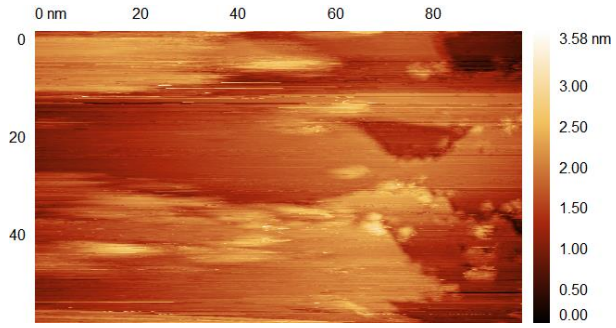


Figure 15: An STM image taken from the location of the transfer on sample 3. Image acquired using the following parameters: $V_{gap}$ = -1 V, loop-gain 1%, $I_t$ = 100 pA, 100.1 nm/s scan speed, 100 × 60 nm$^2$.

STM images from the locations of the transfers on samples 1, 2, and 3 are shown in figures 13, 14 and 15, respectively. The polymer residues in these areas made the measurements very difficult. Scanning in these areas quickly degraded the tip quality. There are a variety of methods for improving tip quality, such as pulsing a voltage over the tip, and scanning on gold [20]. This is of little value though, if the polymer residues are present in sufficient enough quantities, as the tip will degrade before an appreciable area can be scanned. When scanning in the locations of the transfers, the tip would often make large oscillations in height. In order to make a proper comparison of the RMS surface roughness, the areas with wild tip oscillations were cropped out before the calculation. The RMS surface roughness for the areas in figures 13, 14 and 15 was found to be 1.387 nm, 3.148 nm, and 410.0 pm respectively. When comparing the values obtained for the clean and transfer areas, it becomes apparent that 2 min is much too short of a duration for the acetone rinse. Even after rinsing the sample for 2 hours, the location of the transfer was covered with polymer residues to an extent that made it nearly unscannable. It is also apparent that the locations of the transfers contain significantly more residue from the CAB than in the surrounding areas. The surface roughness of the transfer locations were several times higher than the clean areas of the same samples. It is unwise to draw strong conclusions from these measurements as the amount of CAB residue on the surface changed noticeably even within different part of the transfer location. This could explain why sample 2 appeared cleaner than sample 1 in optical microscope images of the transfer locations, but was found to have a higher surface roughness.

## 4.2 Transfer of Graphene and Graphite to GaAs(110)

The fourth sample consisted of graphene and graphite flakes transferred to an undoped GaAs(110) wafer. Optical microscope images of a clean area of the sample and the location of the transfer are shown in figures 16 and 17. Like the other samples, the GaAs had a considerable amount of polymer residue in the location of the transfer, but it appeared to be clean in the other parts of the sample.

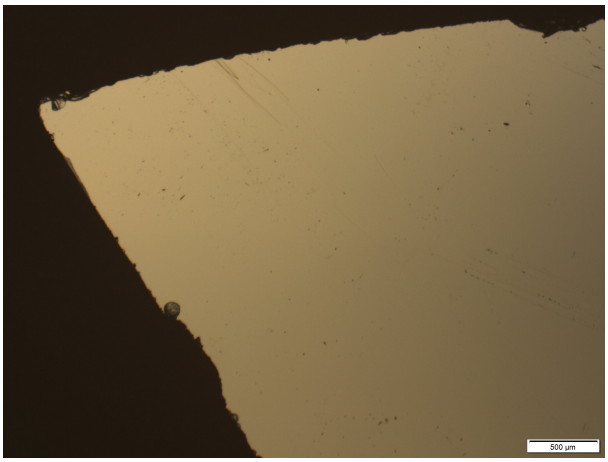


Figure 16: An optical microscope image of a clean area of sample 4, after dissolving away the CAB.

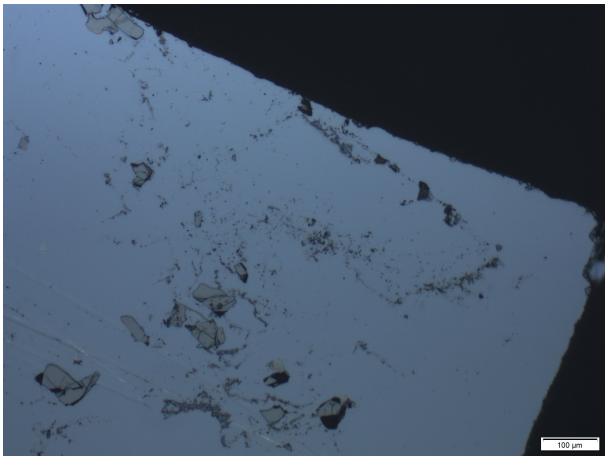


Figure 17: An optical microscope image of sample 4 in the location of the transfer, after dissolving away the CAB.

Figures 18 and 19 are STM images taken of a clean area of sample 4, and the location of the transfer respectively. There was a lot of difficulty in scanning the undoped GaAs sample, even in the clean area. Typically undoped GaAs is illuminated with laser light to excite photocarriers, and increase the tunneling current [29]. The sample was illuminated

by white light, from simple LED lamps that are normally used to illuminate the STM. It is possible that the flux of photons reaching the sample with an energy above the bandgap was not significant enough with this light source, and this may have caused the difficulty with scanning this sample. Even so, this cannot explain away the measurements that were obtained which seem to indicate that the "clean" area is far from clean. The RMS surface roughness was found to be 842.8 pm and 2.378 nm in the areas seen in figures 18 and 19, respectively. Scans in the location of the transfer faced the same trouble as the previous samples, in that polymer residues seemed to adhere and detach from the tip during the scan, causing large oscillations in the height of the tip.

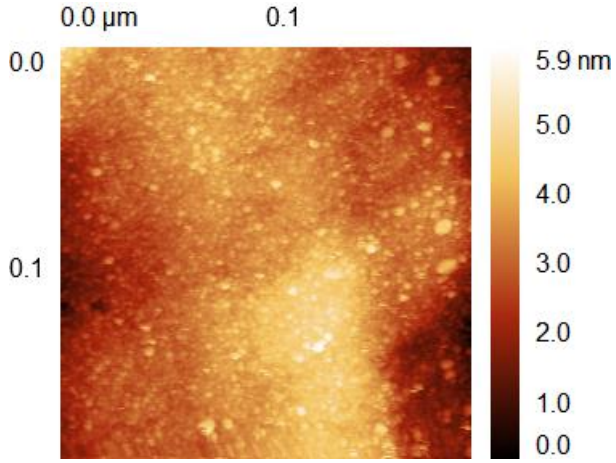


Figure 18: An STM image taken from one of the "clean" areas on sample 4. Image acquired using the following parameters: $V_{gap}$ = -1.5 V, loop-gain 1%, $I_t$ = 100 pA, 100.5 nm/s scan speed, 200 × 200 nm$^2$.

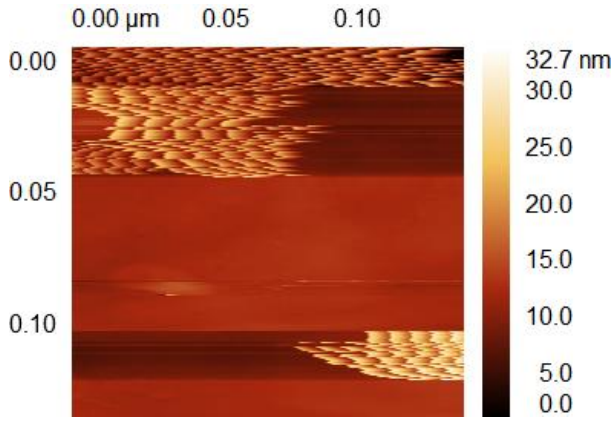


Figure 19: An STM image taken from the location of the transfer on sample 4. Image acquired using the following parameters: $V_{gap}$ = -1.5 V, loop-gain 1%, $I_t$ = 100 pA, 100.5 nm/s scan speed, 150 × 150 nm$^2$.

# 5 Conclusions and Outlook

In short, while we were successful in transferring graphene to InAs(111)B and GaAs(110) using CAB, the transfer process left a significant amount of polymer residue on the surfaces of the samples. The duration for which the samples were cleaned in acetone was extended, but it seemed to have little to no effect on reducing the amount of residue left on the surface. When comparing the RMS surface roughness of the samples, it would appear that the cleaning helps, but it is unwise to draw such a conclusion because in the locations of the transfers, the amount of polymer residue present on the sample changed dramatically from position to position. Still, the areas of the InAs substrate which were not targeted for the transfer remained relatively clean. It is because of this, and the fact that CAB leaves minimal residue on graphene compared with other polymers [19], that there is still value in pursuing the use of CAB for the polymer assisted transfer of graphene to InAs and GaAs nanowires. If a graphene flake is transferred on top of a nanowire, the interface between the graphene and the nanowire will not come into contact with the polymer. The surface of the graphene flake is easily cleaned of the CAB, so if the graphene/nanowire heterostucture can be found in an STM, it should be possible to image the sample without degrading the tip.

Additionally, other researchers have had relatively fewer polymer residues when they used ethyl acetate to dissolve the CAB, and followed it with a rinse in acetone and IPA [19]. It is also possible that CAB is not the best candidate for transfer to InAs and GaAs. Although CAB leaves less residue on graphene, if another polymer, for example PMMA, leaves less residue on the semiconductor substrates, then that may make STM measurements easier and could, ultimately be a better choice. Interestingly, the areas of the GaAs substrate that were not targeted during the transfer, also seemed to be covered in polymer residue. The scans in the "clean" areas were quite rough, and in some places the tip would oscillate rapidly as it did in the locations of the transfers on the other samples. This is possibly because of some unknown reaction between GaAs and the CAB polymer, and thus further studies using other polymers for the transfer are warranted.

There is also the possibility that the graphene should be produced in a different, and more efficient manner that could potentially leave the samples cleaner. Out of more than thirty $Si/SiO_2$ wafers that had graphene/graphite flakes deposited onto them, only three wafers were found to contain graphene flakes of a suitable size ($10\times10$ $\mu$m) to transfer to nanowires for later experiments. Each of these wafers takes roughly 90 minutes to produce and examine under an optical microscope. During this time, many samples could be produced, by for example CVD, requiring much less involvement from a human. This would also have the added benefit that there would be no adhesive residue from tape.

Improving the transfer of graphene will allow for the creation of pristine heterostructures composed of graphene and semiconductors that could revolutionize devices. In one experiment, the photoresponse (the ratio of the photocurrent through a material when illuminated to the photocurrent when in the dark) of InAs nanowires that were stacked on graphene, was investigated. The measured photoresponse was orders of magnitude larger than in graphene alone [3]. Graphene had previously shown promise as a standalone material for photodetectors, but graphene/semiconductor heterostructures may in fact outperform graphene alone. As such, it is not unfathomable that improving transfer techniques of graphene could lead to the development of more efficient devices. Photodetectors operate on a similar principle as LEDs. LEDs have become the primary technology used for lighting, and lighting alone accounted for 15% of global electricity consumption [30]. It is not inconceivable that a breakthrough in the transfer process could lead to the creation of a graphene/semiconductor heterostructure that could significantly reduce the world's energy consumption.

# References


[1] Geim A. Graphene: Status and Prospects. Science. 2009;324(5934):1530-1534.

[2] Novoselov K. Electric Field Effect in Atomically Thin Carbon Films. Science. 2004;306(5696):666-669.

[3] Xie C, Wang Y, Zhang Z, Wang D, Luo L. Graphene/Semiconductor Hybrid Heterostructures for Optoelectronic Device Applications. Nano Today. 2018;19:41-83.

[4] Bostwick A, Ohta T, Seyller T, Horn K, Rotenberg E. Quasiparticle dynamics in graphene. Nature Physics. 2006;3(1):36-40.

[5] Hofmann P. Solid State Physics: An Introduction. 2nd ed. John Wiley and Sons; 2015.

[6] Zhang Z, Yates J. Band Bending in Semiconductors: Chemical and Physical Consequences at Surfaces and Interfaces. Chemical Reviews. 2012;112(10):5520-5551.

[7] Geim A, Novoselov K. The rise of graphene. Nature Materials. 2007;6(3):183-191.

[8] Bolotin, K., Sikes, K., Jiang, Z., Klima, M., Fudenberg, G., Hone, J., Kim, P. and Stormer, H. (2008). Ultrahigh electron mobility in suspended graphene. Solid State Communications, 146(9-10), pp.351-355.

[9] Whitener K, Sheehan P. Graphene synthesis. Diamond and Related Materials. 2014;46:25-34.

[10] Huang Y, Sutter E, Shi N, Zheng J, Yang T, Englund D et al. Reliable Exfoliation of Large-Area High-Quality Flakes of Graphene and Other Two-Dimensional Materials. ACS Nano. 2015;9(11):10612-10620.

[11] Blake P, Hill E, Castro Neto A, Novoselov K, Jiang D, Yang R et al. Making graphene visible. Applied Physics Letters. 2007;91(6):063124.

[12] Li X, Cai W, An J, Kim S, Nah J, Yang D et al. Large-Area Synthesis of High-Quality and Uniform Graphene Films on Copper Foils. Science. 2009;324(5932):1312-1314.

[13] Hao Y, Bharathi M, Wang L, Liu Y, Chen H, Nie S et al. The Role of Surface Oxygen in the Growth of Large Single-Crystal Graphene on Copper. Science. 2013;342(6159):720-723.

[14] Durge R, Kshirsagar R, Tambe P. Effect of Sonication Energy on the Yield of Graphene Nanosheets by Liquid-phase Exfoliation of Graphite. Procedia Engineering. 2014;97:1457-1465.

[15] Hernandez Y, Nicolosi V, Lotya M, Blighe F, Sun Z, De S et al. High-yield production of graphene by liquid-phase exfoliation of graphite. Nature Nanotechnology. 2008;3(9):563-568.

[16] Narita A, Feng X, Müllen K. Bottom-Up Synthesis of Chemically Precise Graphene Nanoribbons. The Chemical Record. 2014;15(1):295-309.

[17] Kang J, Shin D, Bae S, Hong B. Graphene transfer: key for applications. Nanoscale. 2012;4(18):5527.

[18] Caridad J, Power S, Lotz M, Shylau A, Thomsen J, Gammelgaard L et al. Conductance quantization suppression in the quantum Hall regime. Nature Communications. 2018;9(1).

[19] Burwell G, Smith N, Guy O. Investigation of the utility of cellulose acetate butyrate in minimal residue graphene transfer, lithography, and plasma treatments. Microelectronic Engineering. 2015;146:81-84.

[20] Hofmann P. Surface physics. [Place of publication not identified]: Philip Hofmann; 2013.

[21] Mönch W. Semiconductor surfaces and interfaces. 3rd ed. Berlin: Springer; 2013.

[22] Sphalerite-unit-cell-depth-fade-3D-balls.png [Internet]. 2007 [cited 1 May 2020]. Available from: `https://en.wikipedia.org/wiki/Cubic_crystal_system#/media/File:Sphalerite-unit-cell-depth-fade-3D-balls.png`

[23] Hilner E, Lundgren E, Mikkelsen A. Surface structure and morphology of InAs(111)B with/without gold nanoparticles annealed under arsenic or atomic hydrogen flux. Surface Science. 2010;604(3-4):354-360.

[24] Hjort M, Kratzer P, Lehmann S, Patel S, Dick K, Palmstrøm C et al. Crystal Structure Induced Preferential Surface Alloying of Sb on Wurtzite/Zinc Blende GaAs Nanowires. Nano Letters. 2017;17(6):3634-3640.

[25] Blakemore J. Semiconducting and other major properties of gallium arsenide. Journal of Applied Physics. 1982;53(10):R123-R181.

[26] Binnig G, Rohrer H, Gerber C, Weibel E. Surface Studies by Scanning Tunneling Microscopy. Physical Review Letters. 1982;49(1):57-61.

[27] Zhang Y, Qian L, Lai P, Dai T, Liu X. Improved Detectivity of Flexible a-InGaZnO UV Photodetector via Surface Fluorine Plasma Treatment. IEEE Electron Device Letters. 2019;40(10):1646-1649.

[28] Kent T, Edmonds M, Droopad R, Kummel A. InGaAs (110) Surface Cleaning Using Atomic Hydrogen. Solid State Phenomena. 2014;219:47-51.

[29] Takahashi T, Yoshita M, Sakaki H. Scanning tunneling microscopy of undoped GaAs/AlGaAs heterostructures under laser irradiation. Applied Physics Letters. 1996;68(4):502-504.

[30] Rise and Shine: Lighting the World with 10 Billion LED Bulbs [Internet]. Energy.gov. 2020 [cited 1 May 2020]. Available from: https://www.energy.gov/articles/rise-and-shine-lighting-world-10-billion-led-bulbs